Alternating-parity doublets of even-even Ba isotopes

X. Yin,[1] C. Ma,[1] and Y. M. Zhao[1,2,*]

[1]*Shanghai Key Laboratory of Particle Physics and Cosmology, School of Physics and Astronomy, Shanghai Jiao Tong University, Shanghai 200240, China*

[2]*Collaborative Innovation Center of IFSA (CICIFSA), Shanghai Jiao Tong University, Shanghai 200240, China*

(Received 22 October 2023; revised 25 December 2023; accepted 29 January 2024; published 23 February 2024)

In this paper we study the structure of even-even Ba isotopes with neutron number $N = 84$–90 within the framework of nucleon-pair approximation of the shell model. We use a phenomenological Hamiltonian, which includes single-particle energies, monopole, quadrupole, and octupole pairing energies, as well as quadrupole-quadrupole and octupole-octupole interactions. Our calculated energy levels and $B(E2)$ values are in good agreement with experimental data. The alternating parity doublets are well reproduced by considering F^- nucleon pairs with spin-three and negative parity, which demonstrates the importance of F^- pair in octupole deformation. The octupole-octupole interaction is found to favor stronger $B(E3)$ transitions and suppress $B(E2)$ transitions in the low-lying states of nuclei in these even-even Ba isotopes.

DOI: 10.1103/PhysRevC.109.024322

I. INTRODUCTION

Octupole deformation in atomic nuclei has attracted much attention in recent years, as it is quite useful in studies of the electric dipole moment (EDM) problem. The existence of nonzero EDM provides us with direct evidence of charge-parity violation, involving the new physics beyond the standard model of particle physics [1,2]. Experimentally, octupole deformation has been suggested in nuclei ^{220}Rn, ^{222,224,228}Ra [1,3] and ^{144,146}Ba [4,5], where alternating parity rotational bands, large electric octupole transitions, and nonzero electric dipole transitions within the bands were reported. In Ref. [6], the coexistence of quadrupole and octupole deformations was also reported.

From a theoretical point of view, this pear shape is produced by the strong octupole interaction between nucleons in orbits with opposite parity, and with both the orbital and total angular momenta of the two orbits, namely, l and j, differing by $3\hbar$ [7–9]. Thus, pear-shaped nuclei are expected to appear only in specific regions, where proton and/or neutron numbers are close to the so-called 'octupole magic' numbers, 34, 56, 88, and 134 [7]. Theoretically, octupole deformation has been studied in many frameworks, from macroscopic and complex microscopic theories to phenomenological models. In the macroscopic-microscopic models [10,11], the effect of octupole deformation on nuclear ground-state masses was investigated. The study of octupole deformed nuclei by self-consistent mean-field theories can be traced back to the 1980s. Bonche *et al.* used the Hartree-Fock + BCS and generator coordinate method with Skyrme SIII interaction to study the structure of octupole-deformed nuclei [12–14], and Robledo, Egido, and their collaborators carried out a series of studies of octupole deformation with Skyrme and Gogny force within the framework of mean-field theory for several regions of the nuclear chart [15–21]. For completeness, we also list other relevant studies of Refs. [21–33]. A famous phenomenological model, the interacting boson model (IBM) has been extensively applied to study octupole deformation. For example, Engel and Iachello proposed a description of octupole deformation in terms of bosonic U(16) group [34,35]; the importance of p and g bosons in describing $E1$ transitions was pointed out in Refs. [36,37], respectively; in [38,39], it was suggested that octupole deformation arises in the rotational limit; and recently, octupole deformation of specific isotopes near the "octupole magic" number was systematically studied in the framework of sdf-IBM [40–46] based on the nuclear density-functional theory and $spdf$-IBM-2 [47]. Other models, such as reflection-asymmetric relativistic mean-field theory [48], collective models [49–51], cluster models [52,53], and octupole phonon model [54,55], were also used to study the alternating parity rotational bands of octupole-deformed nuclei, as well as the electric octupole and dipole transitions between states of alternating-parity bands.

The nuclear shell model (NSM) is the fundamental theory of nuclear structure. However, the configuration space of the NSM explodes with the numbers of valence nucleons and relevant orbits, therefore truncation to the NSM space is indispensable. Towards this goal, the nucleon-pair approximation (NPA) to the NSM is one natural and efficient truncation scheme. A comprehensive review of the NPA can be found in Ref. [56]. Developments of the NPA in the last two decades can be found in Refs. [57–62]. Clearly, it is interesting to apply the NPA to study the structure of nuclei near the 'octupole magic' numbers. Previously, NPA calculations were performed for nuclei near ^{144}Ba in Refs. [63,64], where states with negative-parity therein were neglected from discussion.

*Corresponding author: ymzhao@sjtu.edu.cn

TABLE I. Single-particle energies (in the unit of MeV) adopted in this paper, taken from Ref. [63].

	$2s_{1/2}$	$1d_{3/2}$	$1d_{5/2}$	$0g_{7/2}$	$0h_{11/2}$	
ϵ_π	2.990	2.690	0.963	0	2.760	
	$1f_{7/2}$	$0h_{9/2}$	$1f_{5/2}$	$2p_{3/2}$	$2p_{1/2}$	$0i_{13/2}$
ϵ_ν	0.000	1.561	2.005	0.854	1.656	1.800

It is therefore the purpose of this paper carrying out a systematic NPA to study the low-lying, both positive and negative parity, states of ^{140,142,144,146}Ba, and to study the effect of octupole deformation.

This paper is organized as follows. In Sec. II, we present a short introduction to the theoretical framework of the NPA, where octupole-octupole interaction is considered in the phenomenological shell model Hamiltonian and a collective F^- nucleon pair is considered in addition to the conventional SD nucleon-pair subspace. In Sec. III, we present our numerical results and discussion. In Sec. IV we summarize this paper.

II. FRAMEWORK

In this section, we present a short discussion of the framework of our NPA calculation. In this paper we use a phenomenological shell-model Hamiltonian as

$$H = \sum_{\sigma=\pi,\nu} (H_0(\sigma) + V(\sigma)) + H_{\pi,\nu}. \tag{1}$$

The first term in Eq. (1) corresponds to the single particle energy,

$$H_0(\sigma) = \sum_{\alpha,\sigma} \epsilon_{\alpha\sigma} C^\dagger_{\alpha\sigma} C_{\alpha\sigma}, \tag{2}$$

where, $\sigma = \pi, \nu$. $\alpha = (nljm)$ denotes all necessary quantum numbers to specify a single-particle state, while $\epsilon_{\alpha\sigma}$ signifies the single-particle energy taken from Ref. [63] and detailed in Table I. The second term in Eq. (1) accounts for residual interactions between like particles. In this paper, we consider the monopole, quadrupole and octupole pairing interactions, along with quadrupole-quadrupole and octupole-octupole interactions. The form of V_σ is

$$V(\sigma) = \sum_{s=0,2,3} G^{(s)}_\sigma \sqrt{2s+1} \big(A^{s\dagger}_\sigma \times \tilde{A}^s_\sigma\big)^{(0)} + \sum_{t=2,3} \kappa^{(t)}_\sigma (-1)^t \sqrt{2t+1} \big(Q^t_\sigma \times Q^t_\sigma\big)^{(0)}. \tag{3}$$

where $A^{s\dagger}_\sigma$ is the collective pair creation operators, defined as

$$\begin{aligned} A^{0\dagger}_\sigma &= \sum_{j_\sigma} \frac{\sqrt{2j_\sigma+1}}{2} \big(C^\dagger_{j_\sigma} \times C^\dagger_{j_\sigma}\big)^{(0)}, \\ A^{2\dagger}_\sigma &= \sum_{j_1 j_2} q(j_1 j_2 2) \big(C^\dagger_{j_{1\sigma}} \times C^\dagger_{j_{2\sigma}}\big)^{(2)}, \\ A^{3\dagger}_\nu &= \big[\big(C^\dagger_{7/2\nu} \times C^\dagger_{13/2\nu}\big)^{3^-} + \big(C^\dagger_{13/2\nu} \times C^\dagger_{7/2\nu}\big)^{3^-}\big], \\ A^{3\dagger}_\pi &= \big[\big(C^\dagger_{5/2\pi} \times C^\dagger_{11/2\pi}\big)^{3^-} + \big(C^\dagger_{11/2\pi} \times C^\dagger_{5/2\pi}\big)^{3^-}\big]. \end{aligned} \tag{4}$$

Q^t_σ is the collective multipole operator defined as

$$Q^t_\sigma = \sum_{j_1 j_2} q(j_1 j_2 t) \big(C^\dagger_{j_{1\sigma}} \times \tilde{C}_{j_{2\sigma}}\big)^{(t)}. \tag{5}$$

The structure coefficients are taken as

$$q(j_1 j_2 t) = (-1)^{j_1+t+1/2} \frac{\sqrt{(2j_1+1)(2j_2+1)}}{\sqrt{4\pi(2t+1)}} \times C^{t0}_{j_1 1/2, j_2 -1/2} \frac{1+(-1)^{l_1+l_2+t}}{2} \langle N_1 l_1 | r^t | N_2 l_2 \rangle. \tag{6}$$

The last term in Eq. (1) corresponds to proton-neutron interaction, and in this paper we take the quadrupole-quadrupole and octupole-octupole type, defined as

$$H_{\pi\nu} = \sum_{t=2,3} \kappa^t_{\pi\nu} (-1)^t \sqrt{2t+1} \big(Q^t_\pi \times Q^t_\nu\big)^0. \tag{7}$$

Our pair-truncated shell-model space is constructed by the coupling proton-pair basis states with neutron-pair basis states. For $2N$ identical nucleons, a nucleon-pair basis state is generated by iteratively coupling collective pairs,

$$|\tau J_N M_N\rangle = ((A^{r_1\dagger} \times A^{r_2\dagger})^{(J_2)} \times \cdots \times A^{r_N\dagger})^{(J_N)} |0\rangle,$$

where $A^{r_i\dagger}$ is a collective nucleon pair,

$$A^{r_i\dagger} = \sum_{j_1 j_2} y(j_1 j_2 r_i) \big(C^\dagger_{j_1} \times C^\dagger_{j_2}\big)^{(r_i)}, \tag{8}$$

where r_i is the spin of collective pair and $y(j_1 j_2 r_i)$ is called structure coefficient.

In this paper, we take collective S^+ (spin-zero with positive parity), D^+ (spin-two with positive parity), and F^- (spin-three with negative parity) pairs for both valence protons and neutrons; Additionally, for ^{144,146}Ba, we include G^+ (spin-four with positive parity) and I^+ (spin-six with positive parity) pairs. Owing to computational resource constraints, the number of G^+, I^+, and F^- pairs is limited to fewer than two for valence protons and valence neutrons, respectively. The structure coefficients $y(j_1 j_2 r_i)$ are determined as follows: S^+ pairs are derived through variation

$$\delta \frac{\langle (S_\pi)^{N_\pi} (S_\nu)^{N_\nu} | \hat{H} | (S_\pi)^{N_\pi} (S_\nu)^{N_\nu} \rangle}{\langle (S_\pi)^{N_\pi} (S_\nu)^{N_\nu} | (S_\pi)^{N_\pi} (S_\nu)^{N_\nu} \rangle} = 0, \tag{9}$$

and non-S pairs are obtained by diagonalizing the Hamiltonian in the subspace of one broken-pair states [65].

III. RESULT AND DISCUSSION

In this paper, strength parameters of the Hamiltonian are obtained by optimizing energy levels of ^{140}Ba, ^{142}Ba, ^{144}Ba, and ^{146}Ba. The resultant parameters are presented in Table II. Figure 1 illustrates the energy ratio for yrast spin-I states with positive parity, compared to the energy of the first 2^+ state. This comparison is based on both experimental data (extracted from the NNDC database [66]) and our calculated results. Additionally, Fig. 2 displays a comparison of low-lying energy levels between experimental data and the NPA calculation.

From Fig. 1, it is evident that both experimental and calculated energy ratios of given I states increase with the neutron number. This observation is understandable because as the neutron number increases, the even-even Ba isotopes

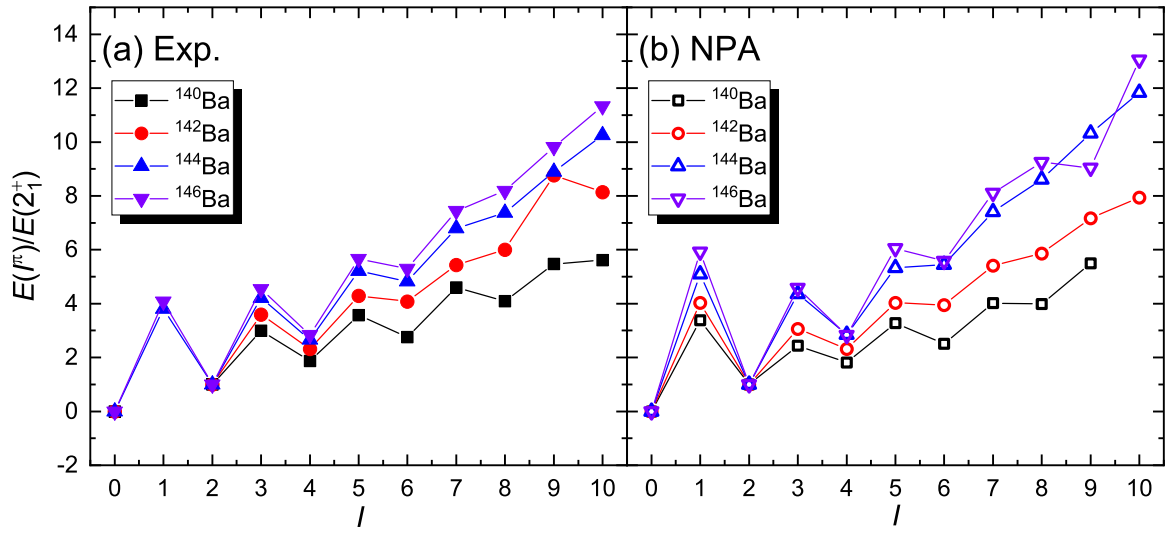

FIG. 1. Energy ratio $E(I^\pi)/E(2_1^+)$ versus I^π, where$\pi = +1$ for even values of I, and $\pi = -1$ for odd values of I. (a), labeled by "Exp.", corresponds to those extracted from experimental data compiled in the NNDC database [66], and (b), labeled by "NPA", corresponds to those calculated by using the nucleon-pair approximation of the shell model in this paper.

become progressively more deformed, as emphasized in Ref. [67]. As for the energies of 2_1^+ states, the calculated values for even-even isotopes ranging from ^{140}Ba to ^{146}Ba are 0.595, 0.358, 0.191, 0.191 MeV, respectively, demonstrating good consistency with the corresponding experimental values of 0.602, 0.359, 0.200, 0.181 MeV. The calculated energy ratios $E(4_1^+)/E(2_1^+)$ presented in Fig. 1(b), are 1.82, 2.33, 2.85, and 2.83, respectively, which align well with the experimental values (1.88, 2.32, 2.66, and 2.84). In this regard, the present calculation enhances the agreement between calculated energy levels and experimental data compared to Refs. [45,63].

In previous studies, alternating parity doublets are employed as a primary feature in the analysis of octupole

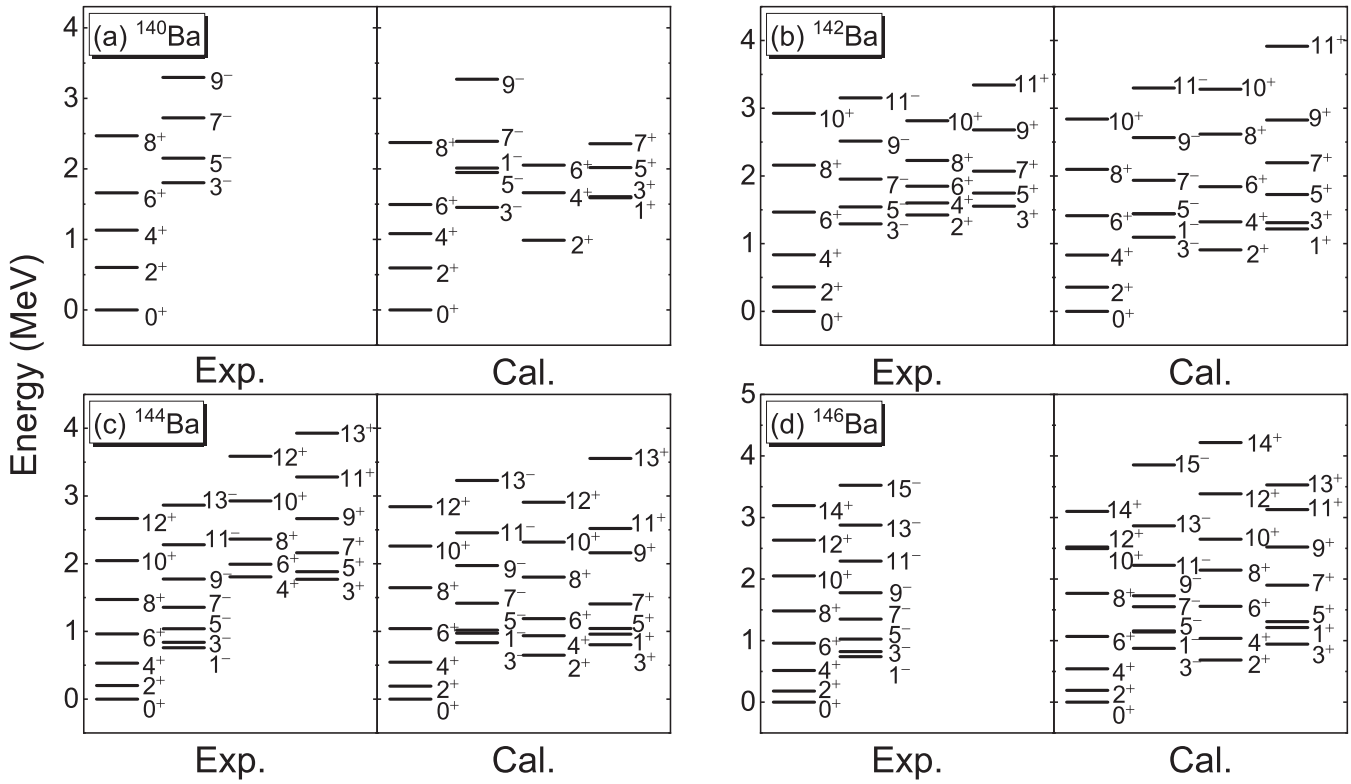

FIG. 2. Experimental and calculated energy levels for ^{140}Ba, ^{142}Ba, ^{144}Ba, and ^{146}Ba. The experimental levels are taken from NNDC [66] and Ref. [6].

TABLE II. Strength parameters of Hamiltonian. In this paper we fix monopole pairing parameters, $G_\pi^{(0)} = -0.13$ MeV, $G_\nu^{(0)} = -0.15$ MeV, and assume smooth values for $\kappa_{\pi\nu}^{(2)}$, $\kappa_{\pi\nu}^{(3)}$ versus the number of valence neutron pairs, N_ν: $\kappa_{\pi\nu}^{(2)} = -0.03 - 0.005N_\nu$ MeV/r_0^4 and $\kappa_{\pi\nu}^{(3)} = -0.005$ MeV/r_0^6. The values of $G_\pi^{(2)}$, $G_\nu^{(2)}$, $\kappa_\pi^{(2)}$, $\kappa_\nu^{(2)}$ (in the unit of MeV/r_0^4), $G_\pi^{(3)}$, $G_\nu^{(3)}$ (in the unit of MeV) and $\kappa_\pi^{(3)}$, $\kappa_\nu^{(3)}$ (in the unit of MeV/r_0^6) are adjusted individually.

	^{140}Ba	^{142}Ba	^{144}Ba	^{146}Ba
$G_\pi^{(2)}$	−0.024	−0.03	−0.036	−0.037
$G_\nu^{(2)}$	−0.015	−0.019	−0.022	−0.028
$\kappa_\pi^{(2)}$	−0.01	−0.015	−0.025	−0.04
$\kappa_\nu^{(2)}$	−0.01	−0.015	−0.025	−0.045
$G_\pi^{(3)}$	−0.45	−0.53	−0.66	−0.70
$G_\nu^{(3)}$	−0.34	−0.43	−0.57	−0.62
$\kappa_\pi^{(3)}$	−0.014	−0.019	−0.022	−0.024
$\kappa_\nu^{(3)}$	−0.008	−0.011	−0.012	−0.013

correlation. For the ideal alternating-parity doublets, the ratio exhibits a quadratic dependence on spin. In the case of octupole vibrational states, the positive parity and negative parity bands remain decoupled, and an odd-even-spin staggering is expected. As illustrated in Fig. 1, both experimental and calculated ratios $E(I_1^\pi)/E(2_1^+)$ ($\pi = +1$ for even values of I, and $\pi = -1$ for odd values of I) increase with spin I in accordance with the odd-even staggering pattern.

Figure 2 presents a comparison between calculated energy levels and corresponding experimental data for even-even $^{140-146}$Ba. One sees a quite good agreement between theoretical calculations and experimental results, with the exception of the calculated energy level of 1_1^- state, which is higher than that of 3^- state, mirroring observations in the *sdf*-IBM calculation as reported in Ref. [45]. This suggests the potential contribution of P^- pair (spin-one with negative parity) to this state. Towards clarification of this observation, studies of core excitation effects is warranted in the future.

In Fig. 3, our calculated energies of 2_1^+–8_1^+ and 1_1^-– 7_1^- states are compared to experimental data and theoretical results of other models, including calculated results by Nomura *et al.* [31] in terms of quadrupole-octupole collective Hamiltonian (QOCH), the IBM results by Nomura *et al.* in Ref. [45], QOCH results calculated by Li *et al.* [27], and calculated results by Jia and collaborators [63] in terms of the NPA. In general, all these calculations yield a correct tendency of evolution of energy levels with respect to neutron number. Yet, the two QOCH calculated energy levels for ^{140}Ba are much higher than corresponding experimental data; the IBM calculated energy levels of 4_1^+–8_1^+ states are also considerably higher than corresponding experimental results. Apparently, calculated results in the present paper are more consistent with experimental data (except for the 1_1^- state). Similarly, in a previous NPA calculation in Ref. [63], only *SD* nucleon pairs were considered and yielded much higher yrast energies for ^{142,144,146}Ba than experimental data.

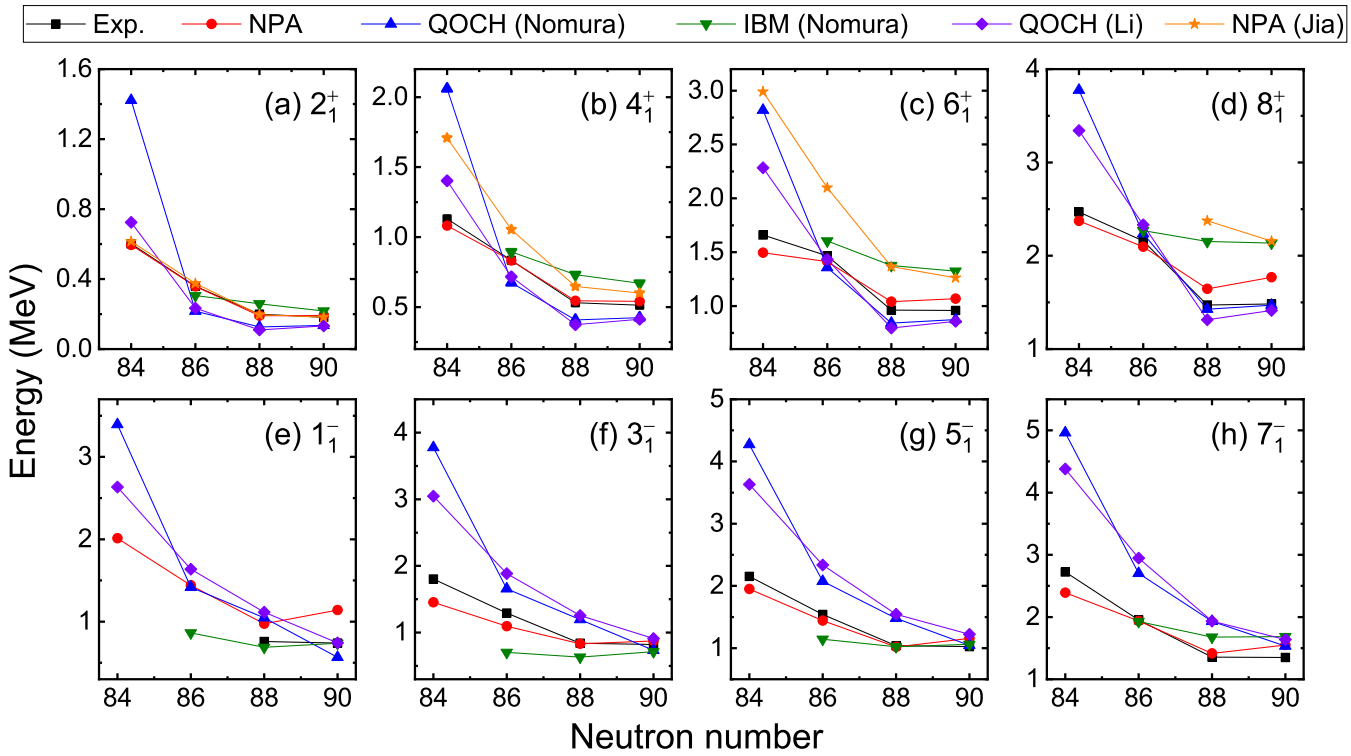

FIG. 3. Energies of 2_1^+, 4_1^+, 6_1^+, 8_1^+ and 1_1^-, 3_1^-, 5_1^-, 7_1^- states versus neutron number. The black squares are the experimental data complied in NNDC. The red circles are the results in this work. Triangles in blue labeled by "QOCH (Nomura)" represent the quadrupole-octupole collective Hamiltonian (QOCH) results by Nomura *et al.* [31], reversed triangles in green labeled by "IBM" represent IBM results also by Nomura *et al.* taken from Ref. [45], diamonds in purple labeled by "QOCH (Li)" represent the QOCH results calculated by Li *et al.* in Ref. [27], and stars in orange labeled by "NPA (Jia)" correspond to NPA results calculated by Jia *et al.* in Ref. [63].

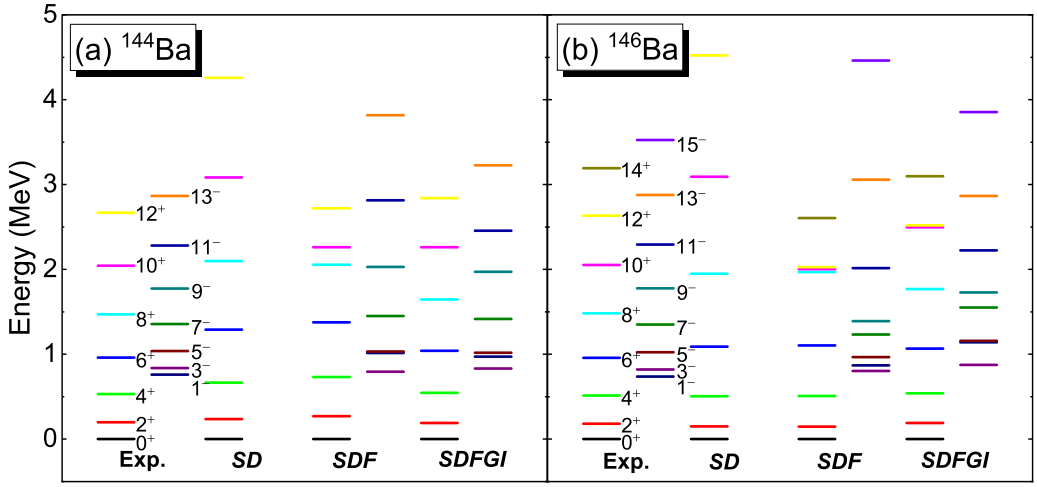

FIG. 4. Low-lying energy levels of ^{144}Ba and ^{146}Ba. "Exp." represents the experimental data taken from the NNDC database. "*SD*" represents the NPA calculation by using *SD* nucleon pairs, "*SDF*" represents the NPA calculation by using *SDF* nucleon pairs, and "*SDFGI*" represents the NPA calculation by using *SDFGI* nucleon pairs.

As Refs. [63,64] only considered S and D pairs in the NPA calculation, it is of interest to investigate the contribution of other nucleon pairs to the even-even Ba isotopes studied in this paper. Figure 4 displays the calculated energy levels of ^{144}Ba and ^{146}Ba by using the NPA calculation in different nucleon-pair configurations, labeled by the "*SD*", "*SDF*", and "*SDFGI*", respectively. As noted earlier, the G^+, I^+, and F^- pairs are less than two for valence protons and valence neutrons, respectively. It can be observed that for ^{144}Ba and ^{146}Ba, the energy levels of 10^+–14^+ in the "*SDF*"-pair calculation are much lower than those of the "*SD*"-pair calculation. This demonstrates that the F^- pair contributes significantly to those states with relatively higher spins; in contrast, the contribution of F^- pair to states with low spins are much smaller. One also sees that for ^{144}Ba, the calculated energy levels of 4^+–8^+ states and 9^-–11^- states in the "*SDFGI*"-pair calculation are lower than those in the "*SDF*"-pair calculation. For ^{146}Ba, the energy levels of the 8^+, 12^+, 14^+ states and 5^-–15^- states in the "*SDFGI*"-pair calculation are more consistent with experimental values than those in the "*SDF*"-pair calculation. These mean that the contribution from G^+ and I^+ pairs are essential for both even-spin positive-parity levels and the odd-spin negative-parity levels of ^{144}Ba and ^{146}Ba.

As for electromagnetic transitions, we use the following transition operators for $E2$ and $E3$ transitions:

$$T(E2) = e_\pi Q_\pi^{(2)} + e_\nu Q_\nu^{(2)},$$
$$T(E3) = e_\pi Q_\pi^{(3)} + e_\nu Q_\nu^{(3)}, \tag{10}$$

where e_π and e_ν are effective charges of valence neutrons and protons that include bare charges, respectively, and corresponding transition strengths $B(E2)$ and $B(E3)$ are

$$B(E2, I_\mathrm{i} \to I_\mathrm{f}) = \frac{2I_\mathrm{f}+1}{2I_\mathrm{i}+1}\langle I_\mathrm{f}||T(E2)||I_\mathrm{i}\rangle^2,$$
$$B(E3, I_\mathrm{i} \to I_\mathrm{f}) = \frac{2I_\mathrm{f}+1}{2I_\mathrm{i}+1}\langle I_\mathrm{f}||T(E3)||I_\mathrm{i}\rangle^2,$$

where I_i, I_f represent the angular momentum of initial and final states, respectively. In this paper, we take the effective charge as $e_\pi = 2.4e$ and $e_\nu = 1.3e$ for both $E2$ and $E3$ transitions.

In Fig. 5, we plot our calculated $B(E2, 2_1^+ \to 0_1^+)$, $B(E3, 3_1^- \to 0_1^+)$ (denoted by NPA) and compare them to all accessible experimental data. As comparison, we also plot results obtained by using other theoretical models, namely the QOCH and the IBM by Nomura *et al.* [31,45], as well as the QOCH results by Li *et al.* [27]. In general, both the magnitudes of $B(E2, 2_1^+ \to 0_1^+)$ and their evolution versus neutron number are satisfactorily reproduced in these models. However, the $B(E3, 3_1^- \to 0_1^+)$ values show significant discrepancies. The measured values are smaller than the experimental values (albeit with large errors).

In Table III we tabulate our calculated $B(E2)$, $B(E3)$ as well as the electric quadrupole moments Q of even-even $^{140-146}$Ba, and compare them with accessible experimental data. One sees good agreement for $B(E2)$ and $Q(2_1^+)$ values. Our calculated $B(E3)$ value reaches its maximum at ^{144}Ba, different from calculated results by using the other models and are thus warranted in future studies. In this study, we also examine the role of octupole-octupole and quadrupole-quadrupole interactions in our calculation. To achieve this, we artificially scale $\kappa_\pi^{(3)}$, $\kappa_\nu^{(3)}$, and $\kappa_{\pi\nu}^{(3)}$ by a parameter α, or scale $\kappa_\pi^{(2)}$, $\kappa_\nu^{(2)}$, and $\kappa_{\pi\nu}^{(2)}$ by a parameter β. In panel (a) of Fig. 6, the resulting $B(E3)$ and $B(E2)$ are plotted against α, while keeping other parameters constant as listed in Table II. It is observed that $B(E3)$ increases with α, while $B(E2)$ decreases with α. Conversely, in panel (b), where $B(E3)$ and $B(E2)$ are plotted against parameter β with other parameters the same as in Table II, one sees that $B(E3)$ decreases while $B(E2)$ increases with β. This indicates that in low-lying states of these nuclei, the octupole-octupole interaction favors stronger $B(E3)$ and reduces the $B(E2)$ values between low-lying states; the quadrupole-quadrupole interaction, on the contrary, favors stronger $B(E2)$ and reduces $B(E3)$ values.

TABLE III. Calculated $B(E2)$ and $B(E3)$ (in the unit of W.u.) and quadrupole moment $Q(2_1^+)$ (in the unit of eb), and corresponding experimental data. Effective charges $e_\pi = 2.4e$, $e_\nu = 1.3e$. Experimental data are taken from the NNDC [66] database and Refs. [4,5,68,69].

	^{140}Ba		^{142}Ba		^{144}Ba		^{146}Ba	
	Exp	Cal	Exp	Cal	Exp	Cal	Exp	Cal
$B(E2, 2_1^+ \to 0_1^+)$	22.4^{+18}_{-47}	24.3	31.8(17)	38.7	48.4^{+16}_{-21}	48.7	60.0(21)	64.3
$B(E2, 4_1^+ \to 2_1^+)$		29.7		54.7	85.7^{+79}_{-74}	71.4	94.4(134)	95.0
$B(E2, 6_1^+ \to 4_1^+)$		21.0		52.7	54.4^{+73}_{-62}	77.2	93.1^{+158}_{-189}	104.7
$B(E2, 8_1^+ \to 6_1^+)$		11.0		40.5	54.6^{+188}_{-123}	50.3	60.6^{+363}_{-184}	105.0
$B(E3, 3^- \to 0_1^+)$		6.5		18.6	49.1^{+256}_{-347}	19.0	47.7^{+205}_{-293}	12.2
$B(E3, 5^- \to 2_1^+)$		5.5		16.9		20.6	73.2^{+883}_{-291}	14.0
$B(E3, 7^- \to 4_1^+)$		2.9		11.6		15.5	82.4^{+1118}_{-445}	11.0
$Q(2_1^+)$	−0.52(34)	−0.287		−0.550		−0.838		−0.986

The above picture for octupole-octupole and quadrupole-quadrupole interactions might be conjectured by intuition, and here, we investigate this scenario in the perspective of occupations in single-particle orbits, both for valence protons and valence neutrons. In Fig. 7, we plot the occupation number in valence orbits versus spin I, where panels (a) and (a′), (b) and (b′), and (c) and (c′) correspond to cases ($\kappa^{(3)} \neq 0$, $\kappa^{(2)} = 0$), ($\kappa^{(3)} \neq 0$, $\kappa^{(2)} \neq 0$), and ($\kappa^{(3)} \neq 0$, $\kappa^{(2)} = 0$), respectively. From panels (a, b) and (a′, b′), respectively, one sees that the occupation number in proton $1d_{5/2}$ and neutron $1f_{7/2}$ orbits decreases with quadrupole-quadrupole interaction switched on. From panels (b, c) and panels (b′, c′), the occupation number of the proton $1d_{5/2}$ and neutron $1f_{7/2}$ orbits increases significantly with octupole-octupole interaction switched on.

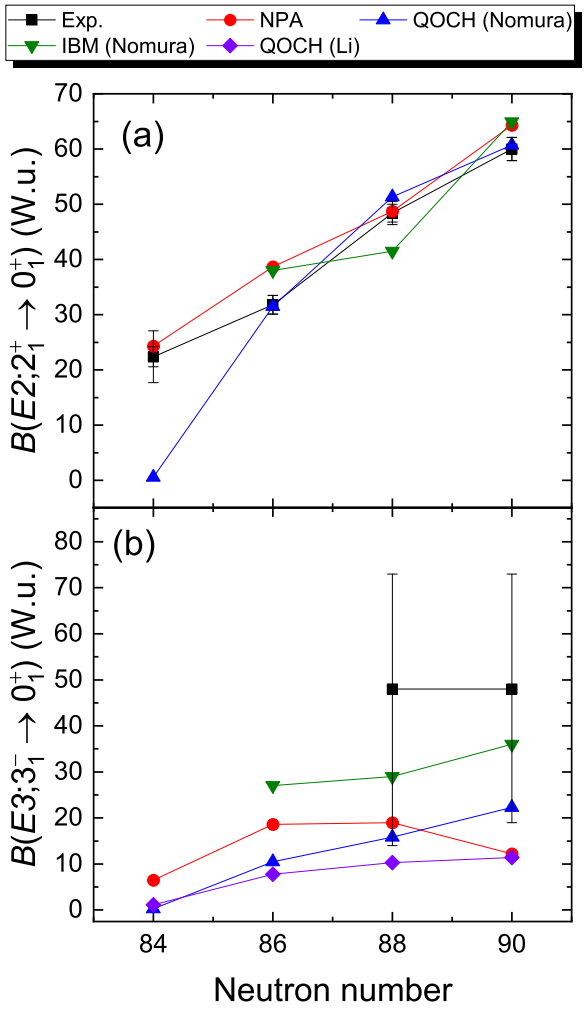

FIG. 5. $B(E2, 2_1^+ \to 0_1^+)$ and $B(E3, 3_1^- \to 0_1^+)$ (in the unit of W.u.) versus neutron number. The notations are the same as in Fig. 3.

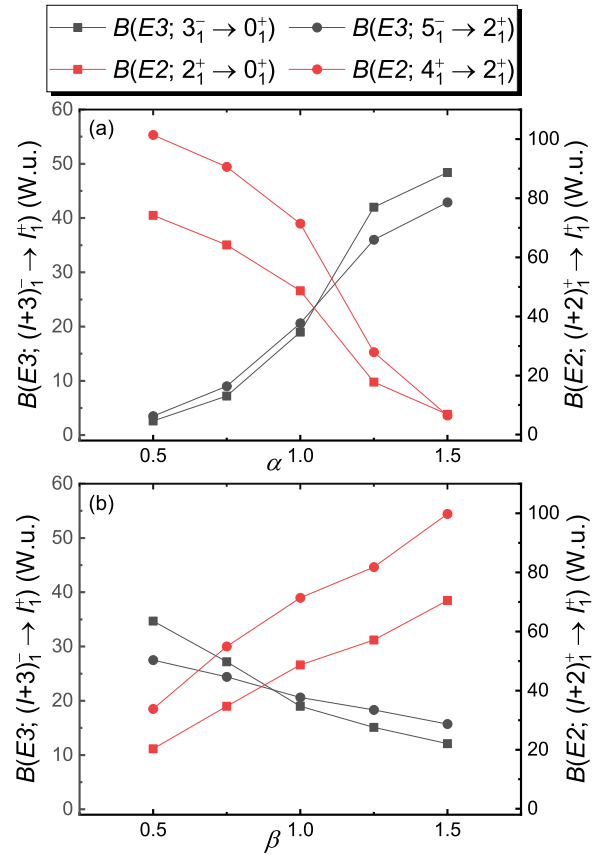

FIG. 6. $B(E3)$ and $B(E2)$ versus α and β, exemplified by using the ^{144}Ba nucleus. (a) $\kappa_\pi^{(3)} = -0.022\alpha$, $\kappa_\nu^{(3)} = -0.012\alpha$, and $\kappa_{\pi\nu}^{(3)} = -0.005\alpha$, with all other parameters the same in Table II; (b) $\kappa_\pi^{(2)} = -0.025\beta$, $\kappa_\nu^{(3)} = -0.025\beta$, and $\kappa_{\pi\nu}^{(2)} = -0.06\beta$, with all other parameters the same in Table II.

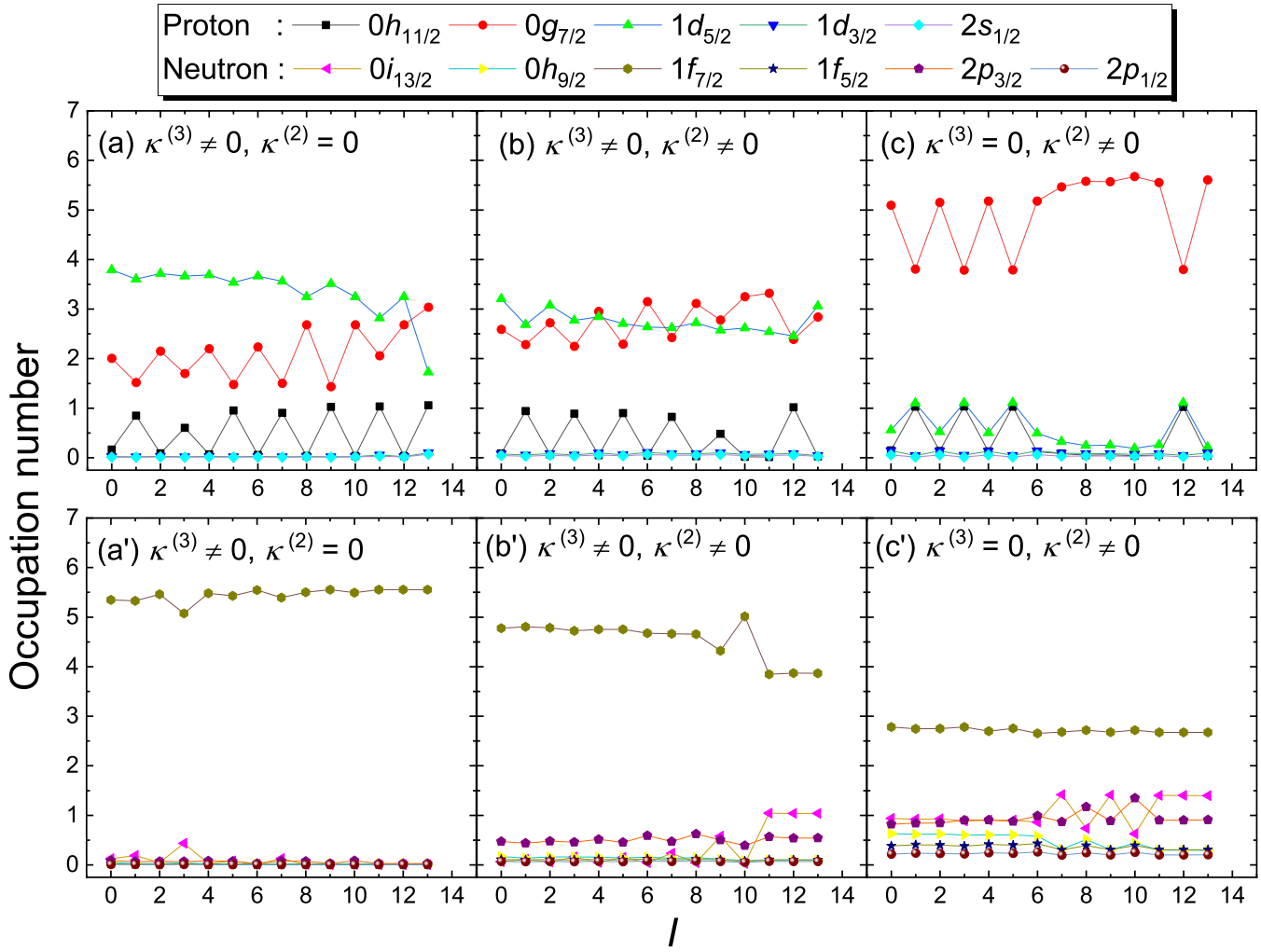

FIG. 7. Occupation number of the orbital members for ^{144}Ba for the case $\kappa^{(3)} \neq 0$ and $\kappa^{(2)} = 0$, corresponding to (a), (d), for the case $\kappa^{(3)} \neq 0$ and $\kappa^{(2)} \neq 0$, corresponding to (b), (e), and for the case $\kappa^{(3)} \neq 0$ and $\kappa^{(2)} = 0$, corresponding to (c), (f).

This is understood from the definition of collective multipole operators, the structure coefficients $q(cdt)$ $(t = 3)$ in Eq. (6) are large only between $1d_{5/2}$ and $0h_{11/2}$ orbits for protons and between $1f_{7/2}$ and $0i_{13/2}$ orbits for neutrons; in contrast, $q(cdt)$ with $(t = 2)$ are considerably large for most orbits with the same parity. Therefore attractive octupole-octupole interaction favors valence protons in the $1d_{5/2}$ orbit and valence neutrons in the $1f_{7/2}$ orbit, while quadrupole-quadrupole interaction relatively favors other orbits. This is also reflected in the pair structure coefficients. In the case with octupole-octupole interaction switched on, our resultant $y(5/2, 5/2, 0)$ and $y(5/2, 5/2, 2)$ for proton SD pairs, and $y(7/2, 7/2, 0)$ and $y(7/2, 7/2, 2)$ for neutron SD pairs, are much larger than those in the case without octupole-octupole interaction. This is very important in reproducing the alternating-parity band structure and considerably large $B(E3)$.

IV. SUMMARY

In this paper, we study the low-lying states of ^{140,142,144,146}Ba within the framework of the nucleon-pair approximation (NPA) of the nuclear shell model, with considerable focus on octupole deformation. We adopt monopole, quadrupole, and octupole pairing interaction plus quadrupole-quadrupole and octupole-octupole interactions. The nucleon-pair subspace is constructed by using spin-three nucleon pairs with negative parity, spin-four, and spin-six nucleon pairs with positive parity, in addition to conventional spin-zero and spin-two SD nucleon pairs, with constraint that the number of nucleon pairs beyond SD subspace exceeds two, neither for valence protons nor valence neutrons. Experimental low-lying energy levels of these nuclei and the $E2$ transition rates between low-lying states are well reproduced in our NPA calculations.

The alternating parity doublets, represented by the energy ratio of $E_{I_1^\pi}/E_{2_1^+}$ versus I, are well reproduced in our calculation. We demonstrate the important roles played by F^- pairs, i.e., nucleon pairs with spin-three and parity-negative, and G^+, I^+ pairs, i.e., nucleon-pairs with spin-four, spin-six, and parity-positive for low-lying states in these nuclei with relatively high spin and low-lying states with negative parity. As in previous studies, the calculated $B(E3)$ values are

systematically smaller than experimental data (albeit with large errors). One possible solution to this deviation might be to consider other interactions which lower down the energies of levels with negative parity in our phenomenological shell model Hamiltonian.

We investigate the roles of quadrupole-quadrupole and octupole-octupole interactions in the $B(E2)$ and $B(E3)$ of low-lying states of these even-even Ba isotopes. We find that the octupole-octupole interaction favors stronger $B(E3)$ and reduces the $B(E2)$ values between low-lying states; the quadrupole-quadrupole interaction, on the contrary, favors stronger $B(E2)$ and reduces $B(E3)$ values. This scenario is also reflected in the occupation numbers of valence protons in the $1d_{5/2}$ orbit and valence neutrons in the $1f_{7/2}$ orbit, as well as in corresponding SD-pair structure coefficients.

ACKNOWLEDGMENTS

We thank the National Natural Science Foundation of China (Grants No. 12375114 and No. 11975151), the Joint Research Program between the HIRFL-CSR mass measurement group in the Institute of Modern Physics, CAS, and the school of Physics and Astronomy in Shanghai Jiao Tong University, and the MOE key Lab for particle Physics, Astrophysics and Cosmology for financial support.

[1] L. P. Gaffney, P. A. Butler, M. Scheck, A. B. Hayes, F. Wenander, M. Albers, B. Bastin, C. Bauer, A. Blazhev, S. Bönig, N. Bree, J. Cederkll, T. Chupp, D. Cline, T. E. Cocolios, T. Davinson, H. De Witte, J. Diriken, T. Grahn, A. Herzan *et al.*, Nature (London) **497**, 199 (2013).
[2] J. Engel, M. J. Ramsey-Musolf, and U. van Kolck, Prog. Part. Nucl. Phys. **71**, 21 (2013).
[3] P. A. Butler, L. P. Gaffney, P. Spagnoletti, K. Abrahams, M. Bowry, J. Cederkall, G. de Angelis, H. De Witte, P. E. Garrett, A. Goldkuhle, C. Henrich, A. Illana, K. Johnston, D. T. Joss, J. M. Keatings, N. A. Kelly, M. Komorowska, J. Konki, T. Kröll, M. Lozano *et al.*, Phys. Rev. Lett. **124**, 042503 (2020).
[4] B. Bucher, S. Zhu, C. Y. Wu, R. V. F. Janssens, D. Cline, A. B. Hayes, M. Albers, A. D. Ayangeakaa, P. A. Butler, C. M. Campbell, M. P. Carpenter, C. J. Chiara, J. A. Clark, H. L. Crawford, M. Cromaz, H. M. David, C. Dickerson, E. T. Gregor, J. Harker, C. R. Hoffman *et al.*, Phys. Rev. Lett. **116**, 112503 (2016).
[5] B. Bucher, S. Zhu, C. Y. Wu, R. V. F. Janssens, R. N. Bernard, L. M. Robledo, T. R. Rodríguez, D. Cline, A. B. Hayes, A. D. Ayangeakaa, M. Q. Buckner, C. M. Campbell, M. P. Carpenter, J. A. Clark, H. L. Crawford, H. M. David, C. Dickerson, J. Harker, C. R. Hoffman, B. P. Kay *et al.*, Phys. Rev. Lett. **118**, 152504 (2017).
[6] S. J. Zhu, E. H. Wang, J. H. Hamilton, A. V. Ramayya, Y. X. Liu, N. T. Brewer, Y. X. Luo, J. O. Rasmussen, Z. G. Xiao, Y. Huang, G. M. Ter-Akopian, and T. Oganessian, Phys. Rev. Lett. **124**, 032501 (2020).
[7] P. A. Butler and W. Nazarewicz, Rev. Mod. Phys. **68**, 349 (1996).
[8] P. A. Butler, J. Phys. G: Nucl. Part. Phys. **43**, 073002 (2016).
[9] P. A. Butler, Proc. R. Soc. A. **476**, 20200202 (2020).
[10] W. Nazarewicz, P. Olanders, I. Ragnarsson, J. Dudek, G. A. Leander, P. Möller, and E. Ruchowsa, Nucl. Phys. A **429**, 269 (1984).
[11] P. Möller, R. Bengtsson, B. G. Carlsson, P. Olivius, T. Ichikawa, H. Sagawa, and A. Iwamoto, At. Data Nucl. Data Tables **94**, 758 (2008).
[12] P. Bonche, P. Heenen, H. Flocard, and D. Vautherin, Phys. Lett. B **175**, 387 (1986).
[13] P. Bonche, S. J. Krieger, M. S. Weiss, J. Dobaczewski, H. Flocard, and P.-H. Heenen, Phys. Rev. Lett. **66**, 876 (1991)
[14] P.-H. Heenen, J. Skalski, P. Bonche, and H. Flocard, Phys. Rev. C **50**, 802 (1994).
[15] L. M. Robledo, J. L. Egido, J. Berger, and M. Girod, Phys. Lett. B **187**, 223 (1987).
[16] L. M. Robledo, J. L. Egido, B. Nerlo-Pomorska, and K. Pomorski, Phys. Lett. B **201**, 409 (1988).
[17] J. L. Egido and L. M. Robledo, Nucl. Phys. A **518**, 475 (1990); **524**, 65 (1991); **545**, 589 (1992).
[18] E. Garrote, J. L. Egido, and L. M. Robledo, Phys. Rev. Lett. **80**, 4398 (1998).
[19] L. M. Robledo and G. F. Bertsch, Phys. Rev. C **84**, 054302 (2011).
[20] R. N. Bernard, L. M. Robledo, and T. R. Rodríguez, Phys. Rev. C **93**, 061302(R) (2016).
[21] R. Rodríguez-Guzmán and L. M. Robledo, Phys. Rev. C **103**, 044301 (2021).
[22] J. Erler, K. Langanke, H. P. Loens, G. Martínez-Pinedo, and P.-G. Reinhard, Phys. Rev. C **85**, 025802 (2012).
[23] S. E. Agbemava, A. V. Afanasjev, and P. Ring, Phys. Rev. C **93**, 044304 (2016).
[24] S. E. Agbemava and A. V. Afanasjev, Phys. Rev. C **96**, 024301 (2017).
[25] Y. Cao, S. E. Agbemava, A. V. Afanasjev, W. Nazarewicz, and E. Olsen, Phys. Rev. C **102**, 024311 (2020).
[26] Z. Xu and Z.-P. Li, Chin. Phys. C **41**, 124107 (2017).
[27] S. Y. Xia, H. Tao, Y. Lu, Z. P. Li, T. Nikšić, and D. Vretenar, Phys. Rev. C **96**, 054303 (2017).
[28] S. Ebata and T. Nakatsukasa, Phys. Scr. **92**, 064005 (2017).
[29] R. Rodríguez-Guzmán, Y. M. Humadi, and L. M. Robledo, Eur. Phys. J. A **56**, 43 (2020).
[30] R. Rodríguez-Guzmán, Y. M. Humadi, and L. M. Robledo, J. Phys. G: Nucl. Part. Phys. **48**, 015103 (2021).
[31] K. Nomura, L. Lotina, T. Nikšić, and D. Vretenar, Phys. Rev. C **103**, 054301 (2021).
[32] J. Yang, J. Dudek, I. Dedes, A. Baran, D. Curien, A. Gaamouci, A. Góźdź, A. Pędrak, D. Rouvel, H. L. Wang, and J. Burkat, Phys. Rev. C **105**, 034348 (2022).
[33] J. Yang, J. Dudek, I. Dedes, A. Baran, D. Curien, A. Gaamouci, A. Góźdź, A. Pędrak, D. Rouvel, and H. L. Wang, Phys. Rev. C **106**, 054314 (2022).
[34] J. Engel and F. Iachello, Phys. Rev. Lett. **54**, 1126 (1985).
[35] J. Engel and F. Iachello, Nucl. Phys. A **472**, 61 (1987).
[36] D. Kusnezov and F. Iachello, Phys. Lett. B **209**, 420 (1988).
[37] N. Yoshinaga, T. Mizusaki, and T. Otsuka, Nucl. Phys. A **559**, 193 (1993).
[38] N. V. Zamfir and D. Kusnezov, Phys. Rev. C **63**, 054306 (2001).

[39] N. V. Zamfir and D. Kusnezov, Phys. Rev. C **67**, 014305 (2003).
[40] K. Nomura, D. Vretenar, and B.-N. Lu, Phys. Rev. C **88**, 021303(R) (2013).
[41] K. Nomura, D. Vretenar, T. Nikšić, and B.-N. Lu, Phys. Rev. C **89**, 024312 (2014).
[42] K. Nomura, R. Rodriguez-Guzmán, and L. M. Robledo, Phys. Rev. C **92**, 014312 (2015).
[43] K. Nomura, R. Rodríguez-Guzmán, Y. M. Humadi, L. M. Robledo, and J. E. Garcia-Ramos, Phys. Rev. C **102**, 064326 (2020).
[44] K. Nomura, R. Rodriguez-Guzmán, L. M. Robledo, and J. E. García-Ramos, Phys. Rev. C **103**, 044311 (2021).
[45] K. Nomura, R. Rodriguez-Guzmán, L. M. Robledo, J. E. García-Ramos, and N. C. Hernández, Phys. Rev. C **104**, 044324 (2021).
[46] K. Nomura, Phys. Rev. C **105**, 054318 (2022).
[47] O. Vallejos and J. Barea, Phys. Rev. C **104**, 014308 (2021).
[48] Y.-T. Qiu, X.-W. Wang, and J.-Y. Guo, Phys. Rev. C **106**, 034301 (2022).
[49] D. Bonatsos, D. Lenis, N. Minkov, D. Petrellis, and P. Yotov, Phys. Rev. C **71**, 064309 (2005).
[50] D. Lenis and D. Bonatsos, Phys. Lett. B **633**, 474 (2006).
[51] P. G. Bizzeti and A. M. Bizzeti-Sona, Phys. Rev. C **88**, 011305(R) (2013).
[52] T. M. Shneidman, G. G. Adamian, N. V. Antonenko, R. V. Jolos, and W. Scheid, Phys. Lett. B **526**, 322 (2002).
[53] T. M. Shneidman, G. G. Adamian, N. V. Antonenko, R. V. Jolos, and W. Scheid, Phys. Rev. C **67**, 014313 (2003).
[54] N. Yoshinaga, K. Yanase, K. Higashiyama, and E. Teruya, Phys. Rev. C **98**, 044321 (2018).
[55] N. Yoshinaga, K. Yanase, C. Watanabe, and K. Higashiyama, Prog. Theor. Exp. Phys. **2021**, 063D01 (2021).
[56] Y. M. Zhao and A. Arima, Phys. Rep. **545**, 1 (2014).
[57] Y. M. Zhao, N. Yoshinaga, S. Yamaji, J. Q. Chen, and A. Arima, Phys. Rev. C **62**, 014304 (2000).
[58] H. Jiang, Y. Lei, C. Qi, R. Liotta, R. Wyss, and Y. M. Zhao, Phys. Rev. C **89**, 014320 (2014).
[59] G. J. Fu, Y. Lei, Y. M. Zhao, S. Pittel, and A. Arima, Phys. Rev. C **87**, 044310 (2013).
[60] Y. Y. Cheng, Y. M. Zhao, and A. Arima, Phys. Rev. C **97**, 024303 (2018).
[61] Y. Lei, Y. Lu, and Y. M. Zhao, Chin. Phys. C **45**, 054103 (2021).
[62] C. Ma, X. Yin, and Y. M. Zhao, Phys. Rev. C **108**, 034308 (2023).
[63] L. Y. Jia, H. Zhang, and Y. M. Zhao, Phys. Rev. C **75**, 034307 (2007).
[64] L. Y. Jia, H. Zhang, and Y. M. Zhao, Phys. Rev. C **76**, 054305 (2007).
[65] Z. Y. Xu, Y. Lei, Y. M. Zhao, S. W. Xu, Y. X. Xie, and A. Arima, Phys. Rev. C **79**, 054315 (2009).
[66] National Nuclear Data Center, https://www.nndc.bnl.gov/.
[67] J. B. Gupta and M. Saxena, Phys. Rev. C **91**, 054312 (2015).
[68] C. Bauer, T. Behrens, V. Bildstein, A. Blazhev, B. Bruyneel, J. Butterworth, E. Clement, L. Coquard, J. L. Egido, A. Ekström, C. R. Fitzpatrick, C. Fransen, R. Gernhaeuser, D. Habs, H. Hess, J. Leske, T. Kroell, R. Kruecken, R. Lutter, and A. Wiens, Phys. Rev. C **86**, 034310 (2012).
[69] S. Raman, C. W. Nestor, Jr., and P. Tikkanen, At. Data Nucl. Data Tables **78**, 1 (2001).